Transcriptome-wide Landscape of RNA Modification N^6-Methyladenosine in Chromophobe Renal Cell Carcinoma

Zhigang Chen
Peking University Third Hospital
Junbo Yang
Peking University College of Chemistry and Molecular Engineering
Wei Zhang
Peking University College of Chemistry and Molecular Engineering
Yang Qian
Peking University College of Chemistry and Molecular Engineering
Nan Zhang
Peking University College of Chemistry and Molecular Engineering
Zixin Chen
Peking University College of Chemistry and Molecular Engineering
Min Lu
Peking University Third Hospital
Liyuan Ge
Peking University Third Hospital
Cheng Liu
Peking University Third Hospital
guifang Jia (guifangjia@pku.edu.cn)
Peking University https://orcid.org/0000-0002-4186-6922
Lulin Ma
Peking University Third Hospital

Primary research

Keywords: chromophobe renal cell carcinoma, N6-methyladenosine, RNA modifiction

Posted Date: June 24th, 2021

DOI: https://doi.org/10.21203/rs.3.rs-641341/v1

Abstract

Background

As the most abundant internal mRNA modification, N^6-methyladenosine (m^6A) is associated with various cancers. However, RNA modification m^6A has not been studied in chromophobe renal cell carcinoma (chRCC). The present study aimed to comprehensively analyze the global m^6A modification pattern in chRCC.

Methods

Three subjects with chRCC were enrolled in our study. Transcriptome-wide m^6A methylone and transcriptome analysis in chRCC and tumor-adjacent normal tissues were detected via m^6A-SEAL-seq and RNA-sEq. m^6A-modified mRNAs were further validated by m^6A-immunoprecipition followed by quantitative real-time PCR (m^6A-IP-qPCR). The least absolute shrinkage and selection operator (LASSO) Cox regression and multivariate Cox proportional hazards regression analysis were used to determine the candidate gene.

Results

We performed qPCR in six subjects of chRCC and found that the expression levels of m^6A writer subunit WTAP, m^6A erasers FTO and ALKBH5, and m^6A reader YTHDF2 were significantly downregulated in chRCC tissues compared with corresponding tumor-adjacent normal tissues. In all three subjects, 12,841 confident m^6A peaks representing 10,102 transcripts and 15,024 confident m^6A peaks representing 11,396 transcripts were respectively identified in chRCC and tumor-adjacent normal tissues. Analysis of differential m^6A levels identified 644 hypermethylated m^6A peaks and 1,304 hypomethylated m^6A peaks in chRCC compared with tumor-adjacent normal tissues. Gene Ontology (GO) analysis revealed that genes with hypomethylated m^6A peaks (1,137) were associated with pathways in cancer. Compared with tumor-adjacent normal tissues, 3,911 genes were significantly dysregulated in chRCC, including 2,344 downregulated and 1,567 upregulated mRNAs. Functional enrichment analysis revealed that the dysregulated genes in chRCC were significantly enriched in multiple metabolic processes. We identified two hypomethylated genes NOTCH1 and FGFR1, which might respectively act as a tumor suppressor and an oncogene in chRCC. Three m^6A-dependent signatures were identified using Cox regression screen and LASSO regression. Based on the significant prognostic signatures, we build a m^6A-dependent prognostic model, with the Concordance index (C-index) = 0.96. The Kaplan-Meier survival curve and log-rank between the high-risk and low-risk group showed significant difference.

Conclusions

This study presented the first m^{6}A transcriptome-wide profile of human chRCC, which may provide clues for the m^{6}A methylation-based research on chRCC epitranscriptomic etiology and pathogenesis.

Background

According to the Global Cancer Observatory (GCO) database (2020), there are more than 431 thousand kidney cancer incidence and more than 179 thousand people died due to kidney cancer all of the world. Kidney cancer remains a high occurrence (15th) and a leading cause of cancer-related deaths (16th). The molecular mechanisms of kidney cancer progression need to be solved urgently. There are three main types of kidney cancer: clear cell renal cell carcinoma (ccRCC), papillary renal cell carcinoma (PRCC), and chromophobe renal cell carcinoma (chRCC). ccRCC is the most prevalent type of kidney cancer and has been improved in pathogenesis and therapy [1–4]. PRCC is the second most common type of renal carcinoma and also a well-studied type of renal cell carcinoma (RCC) currently [5, 6]. Whereas chRCC is an uncommon RCC subtype, accounting for 5–10% of all cases of RCC [7]. Previous studies suggest that the clinical symptoms of chRCC are not typical. Surgery is the dominant treatment method, and currently there is no standard treatment regimen for metastatic patients. With early diagnosis, chRCC can be curable by surgery [8, 9]. However, chRCC is still a malignant neoplasm with a mortality rate about 10%, and aggressive clinical course such as metastasis can occur [10]. Therefore, the study of chRCC will contribute to the understanding of kidney cancer progression.

According to the RNA modification database, more than 170 types of modifications have been identified in RNA molecule [11]. N^6-methyladenine (m^{6}A) is the most abundant mRNA modification in eukaryotes and plays important roles in various biological functions including regulation of RNA stability [12–14], 3'-end processing [15, 16], alternative splicing [17, 18], and translation efficiency at the post-transcriptional level [14, 19, 20]. m^{6}A is a dynamically reversible RNA modification, which is regulated by “writers” (methyltransferases), “erasers” (demethylases), and “readers” (binding proteins). The majority of m^{6}A modifications are installed through the methyltransferase complex containing key catalytic subunits METTL3-METTL14 heterodimer [21, 22] and other subunits like WTAP [23–25], and removed by demethylases like FTO and ALKBH5 [26, 27]. m^{6}A modification is recognized by m^{6}A binding proteins, such as YTH domain family proteins, for regulation of RNA processing and metabolism [28–30]. The discoveries of these different m^{6}A regulators contribute to a better understanding of the physiological functions of m^{6}A.

Numerous studies have demonstrated a close relationship between m^{6}A modification and tumor progression [31–34]. For instance, in bladder cancer, METTL3 installs m^{6}A in pri-miR221/222 and accelerates the maturation of miRNAs, leading to the proliferation of cancer cell [35]. In pancreatic cancer, ALKBH5 inhibits cancer cell growth and progression through increasing *PER1* mRNA levels by demethylating m^{6}A modification in *PER1* and subsequently escaping from YTHDF2-mediated mRNA decay [34]. These findings suggest that m^{6}A modification plays vital roles in carcinogenesis through the regulation of RNA processing and metabolism and provide new molecular mechanisms of cancer

progression. Similarly, m^6A regulators also have significant impacts on ccRCC [36]. METTL14 is downregulated in ccRCC tissue and patients with lower METTL14 expression tend to have worse prognoses [37], and the alteration of m^6A regulators is associate with worse clinical characteristics [38]. In RPCC, a prognostic risk signature model with three m^6A regulatory genes, IGF2BP3, KIAA1429 and HNRNPC, could predict survival outcomes accurately [39]. With the development of high-throughput sequencing, transcriptome-wide profiling of m^6A distribution in multiple different human carcinomas becomes available, which gives a way to interpret the molecular mechanisms between m^6A modification and RCC. In 2020, transcriptome-wide m^6A mapping in ccRCC were reported, and the unique m^6A-related genes in ccRCC are associated with cancer-related pathways, providing a possible mechanism of m^6A-mediated gene regulation [40]. However, the transcriptome-wide distribution of m^6A in chRCC has not been figured out yet. Here, we report the transcriptome-wide m^6A profiling in human chRCC by the use of antibody-free methods m^6A-SEAL-seq [41], which is a FTO-assisted chemical labeling m^6A sequencing method and has good sensitivity, specificity and reliability. This study will be helpful for providing a basis for more in-depth studies of the biological functions of m^6A in pathogenesis of human chRCC.

Methods

Patients and specimens

A total of six patients with chRCC were involved in our study. chRCC tissues and corresponding tumor-adjacent normal tissues were collected at the time of surgery from urology department, Peking University Third Hospital. All specimens were immediately separated into 1.5 ml RNase-free centrifuge tubes and stored at -80 °C before RNA isolation.

RNA Preparation

Total RNA was extracted from tissue specimens using TRIzol reagent (Magen) and poly(A)$^+$ RNA was isolated from total RNA using oligo(dT) 25 Dynabeads (Thermo Fisher Scientific). RNA concentration was determined using a Nanodrop ultraviolet-visible light spectrophotometer (Thermo).

m^6A-SEAL-seq and library construction

Poly(A)$^+$ RNA isolated from each sample was fragmented by a magnesium RNA fragmentation module (NEB) and subjected in FTO-assisted m^6A oxidation step. In FTO-assisted m^6A oxidation step, the reaction was performed in 300 μl aliquots of aqueous solution containing 300 μM of $(NH_4)_2Fe(SO_4)_2{\cdot}6H_2O$, 2 mM of L-ascorbic acid, 300 μM of α-KG, 100 mM pH 7.0 HEPES, 0.2 μM FTO, and 1 μg poly(A)$^+$ RNA. After the FTO treatment at 37 °C for 5 min, RNA was purified by Oligo Clean & Concentrator column (Zymo Research).

hm^6A-modified RNA converted from m^6A by FTO oxidation was treated by 200 mM freshly prepared DTT at 37 °C for 3 h in acidic aqueous solution (100 mM HEPES, pH 4.0). The product RNA was purified by

ethanol precipitation.

After ethanol precipitation, DTT-treated RNA was washed by 75% ethanol and dissolved in 200 µl biotinylation buffer that contained 100 µM of MTSEA-XX-biotin (Biotum), 100 mM HEPES (pH 7.0), 1 mM EDTA, and 20% DMF. The reaction was performed at 25 °C and 800 rpm in a ThermoMixer for 1 h. The biotinylated RNA was purified by phenol-chloroform extraction.

50 ng of the biotinylated RNA was saved as input, and the rest was proceeded to affinity enrichment. 20 µl Dynabeads MyOne Streptavidin C1 (Invitrogen) was washed twice by 200 µl 0.1 M NaOH to remove RNase contamination, and then washed with diethyl pyrocarbonate water to a neutral pH. The beads were resuspended in 100 µl binding solution containing 10 µl of high-salt wash buffer (100 mM Tris pH 7.5, 10 mM EDTA, 1 M NaCl, 0.05% Tween 20) and 90 µl diethyl pyrocarbonate water, and incubated with the biotinylated RNA for 1 h. The biotinylated RNA on beads was washed three times with 1 ml high salt wash buffer. 50 µl of 100 mM DTT was used to release the biotinylated RNA at 37 °C for 15 min on a ThermoMixer (800 rpm.). After collecting the supernatant, the second elution was performed with 50 µl of 100 mM DTT at 50 °C for 5 min to completely release the RNA. The twice-eluted RNA was combined and purified by ethanol precipitation. Library construction was performed using NEBNext Ultra II Directional RNA Library Prep Kit for Illumina according to the manufacturer's protocol. Libraries were sequenced on the Illumina HiSeq XTen platform with a paired-end model (PE150).

Analysis of m^6A-seq data

Sequencing reads were trimmed and mapped to the reference genome (GRCh38) by using Cutadapt (v1.18) [42] and HISAT2 (v2.1.0) [43], respectively. The m^6A-enriched regions in chRCC and normal tissues were identified using the MACS2 [44] peak-calling algorithm based on enrichment criteria (IP/Input) ≥ 2 and FDR < 0.05. Confident m^6A peaks were subjected to Hypergeometric Optimization of Motif EnRichment tools (HOMER) [45] for Motif Discovery. Genes with differentially methylated m^6A sites were identified by MeTDiff [46] based on enrichment criteria fold change ≥ 2 and FDR < 0.05. Tissue analysis, Gene ontology (GO) and pathway enrichment analyses were performed by using DAVID.

Analysis of RNA-seq data

Adapter and low-quality reads were trimmed by using Cutadapt (v1.18) [42], and trimmed reads were aligned to the reference genome (GRCh38) using HISAT2 (v2.1.0) [43]. The differential expression genes between chRCC and adjacent normal tissues were screened by R package (DEseq2) [47] based on a cutoff criterion of fold change ≥ 2 and FDR < 0.05.

Risk stratification and survival analysis

A cohort of 65 chRCC cases from The Cancer Genome Atlas (TCGA) database was used to illustrate the relationship between the differential expressed DMMGs and chRCC patients. We randomly chose 40 samples from 65 cases as a training set to predict signature model and the rest samples form a testing

set to verify the model (make sure the training set and testing set both contain tumor samples and normal samples). Firstly, we used least absolute shrinkage and selection operator (LASSO) to select candidate genes (glmnet package) in training set. Secondly, we performed the multi-variates cox regression and removed genes not supported by PH hypothesis using the selected candidate genes in training set. Thirdly, we performed the second regression (survival package) to calculate the coefficients between candidate genes and 5-years survival using the remaining candidate genes in training set to build a Cox model. The concordance index (C-index) was calculated to evaluate the prognostic power. Risk score of each sample was calculated through the sum of the product of each candidate gene fpkm-uq and its coefficient in training set. The patients were then classified into high-risk or low-risk group using the risk score where the difference value of true positive and false positive reaches to the maximum as the cutoff value. The Kaplan-Meier survival curve (survminer package) was performed to evaluate the 5-years survival, and the sensitivity and accuracy of the cox model to predict clinical outcome were evaluated by the area under curve (AUC) of the receiver operating characteristic (ROC) curve (survival ROC package). At last we test the signature model in the testing set, ccRCC dataset (a cohort of 602 cases from TCGA database) and PRCC dataset (a cohort of 318 cases from TCGA database).

Results

The aberrant expression of several m^{6}A regulators in chRCC tissue

Hematoxylin–eosin (HE) staining indicated that chRCC tissues composed of large vegetable-like polygonal cells with eosinophilic cytoplasm, irregular nuclei, perinuclear clear halo, and prominent cell membrane (Fig. 1b). In order to determine whether m^{6}A modification functions in chRCC, we first analyzed the expression levels of 8 m^{6}A regulators, including 3 key writer subunits, 3 readers, and 2 erasers (m^{6}A writer subunits: METTLE14, METTL3, and WTAP; m^{6}A readers: YTHDF1, YTHDF2, and YTHDF3; m^{6}A erasers: ALKBH5 and FTO) in six patients. The qPCR results showed that the expression levels of WTAP, YTHDF2, FTO, and ALKBH5 were downregulated markedly in chRCC tissues compared with corresponding tumor-adjacent normal tissues (termed normal tissues) (Fig. 1c). The aberrant expression of these m^{6}A regulators in chRCC indicated that m^{6}A modification might play a crucial role in the progression of chRCC.

Overview of m^{6}A methylation feature in normal and chRCC tissues

To investigate whether m^{6}A methylation landscape changes between the normal and chRCC tissues, we performed m^{6}A-SEAL-seq [41] using chRCC tissues and normal tissues from three subjects. Approximately 87.1-13.2 million reads were generated from each library and 82.8-12.8 million reads were mapped to GRCh38 genome (Additional file 1: Dataset S1). m^{6}A peaks were called in each sample using the published m^{6}A peak caller MACS2 algorithm [44] (fold enrichment (IP/input) ³ 2 and false discovery rate (FDR) £ 0.05). The m^{6}A peaks identified in all three replicates were classified as “confident m^{6}A peaks”. We identified 15,024 confident m^{6}A peaks corresponding to 11,396 transcripts/genes in normal

tissues, and 12,841 confident m^{6}A peaks corresponding to 10,102 transcripts/genes in chRCC tissue (Fig. 2a). To evaluate the reliability and performance of m^{6}A-SEAL-seq, we compared our confident m^{6}A peaks identified in normal tissues with the published m^{6}A peaks identified in normal kidney tissues by MeRIP-seq (GSE122744) [48]. 5686 out of 7261 (78.3%) of the m^{6}A peaks in MeRIP-seq were overlapped with our identified m^{6}A peaks in m^{6}A-SEAL-seq (Additional file 2: Fig. S1a). We then plotted the distribution of distance between m^{6}A peaks from m^{6}A-SEAL-seq and MeRIP-seq, and found that our confident m^{6}A peaks were highly enriched around MeRIP-seq peaks (Additional file 2: Fig. S1b). We further calculated normalized read coverages from m^{6}A-SEAL-seq around MeRIP-seq peaks by deepTools [49]. Their co-enrichment was further shown in Supplementary Figure 1C and 1D. These results suggest that m^{6}A-SEAL-seq is accurate and reliable.

We next investigated the m^{6}A distribution across transcripts in normal and chRCC tissues. The metagene profiles was used to display the distribution of m^{6}A peaks across transcripts. The results showed that confident m^{6}A peaks in normal and chRCC tissues were both highly located within coding sequences (CDS) and 3' untranslated region (3'UTR) (Fig. 2b), which was consistent with the previous observation [40]. To further locate confident m^{6}A peaks, we divided the transcripts into five non-overlapping regions and assigned the confident m^{6}A peaks into these regions. The fraction of confident m^{6}A peaks of normal and chRCC tissues in these five regions showed that they were dominantly enriched in 3'UTR (40.46%, 40.55%), CDS (29.01%, 26.54%) and stop codon (17.32%, 18.59%) (Fig. 2c). We clustered the confident m^{6}A peaks in HOMER (Hypergeometric Optimization of Motif Enrichment) software [45] and found the motif GGACH (H=U>A/C) in normal tissue and WRAC (W=G>C, R=G>A), RAACW (R=G>A, W=U>A) in chRCC tissue (Supplementary Figure 3), which are similar to the known m^{6}A motif, RRACH (R=G/A, H=A/C/U).

Further we asked which RNA molecules prefer to contain m^{6}A modification. We assigned confident m^{6}A peaks to GRCh38 genome and found that 76.24% and 77.78% were mRNA, 18.42% and 17.16% were long non-coding RNA (lncRNA) in normal and chRCC tissues, respectively (Fig. 2d). We noticed that the confident m^{6}A peaks number in chRCC tissues were less than that in normal tissues (Fig. 2a). We subsequently assigned m^{6}A peaks to chromosome, genes and the five non-overlapping regions. We found that the number of confident m^{6}A peaks in chRCC tissues were decreased globally among each chromosome except chromosome Y, which didn't have m^{6}A peaks (Fig. 2e). By analyzing the distribution of m^{6}A peaks per gene, we found that most of m^{6}A-motified mRNAs contained one or two m^{6}A peak, while a small number of them contained three or more (Fig. 2f), consistent with previous studies such as ccRCC [40]. In each group of m^{6}A peaks per gene, chRCC tissues always contain less gene number than normal tissues (Fig. 2f). We also counted the number of m^{6}A peaks among the five non-overlapping regions in normal and chRCC tissues and found that chRCC tissues contain less m^{6}A peak numbers in 3'UTR, 5'UTR, CDS, and stop codon compared with normal tissues (Fig. 2g). These results suggest that m^{6}A modification level decreased in chRCC tissues.

Differentially methylated m^{6}A genes (DMMGs) participate in multi-cancer related pathways

To dissect the role of m^{6}A modification, we subsequently identified differentially methylated m^{6}A peaks (DMMPs) between normal and chRCC tissues using the MeTDiff R package software [46] (p £ 0.05). We identified 644 hypermethylated m^{6}A peaks representing 593 transcripts and 1,304 hypomethylated m^{6}A peaks representing 1,137 transcripts in chRCC tissues of all three subjects compared with normal tissues (Fig. 3a). Recall that our qPCR results in six subjects of chRCC showing that m^{6}A writer subunit WTAP and m^{6}A erasers FTO and ALKBH5 were significantly downregulated in chRCC (Fig. 1c), the identified hypomethylated m^{6}A and hypermethylated m^{6}A sites in chRCC could be directly induced by the aberrant expression of WTAP and FTO/ALKBH5, respectively. The identified hyper- and hypomethylated m^{6}A peaks in chRCC tissues were respectively regarded as hyper and hypo group. Motif search analysis using HOMER revealed one overrepensented motif GGACH (H=U>C/A) in hypermethylated m^{6}A peaks and two highly enriched motifs GGAC and GAACU in hypomethylated m^{6}A peaks; all these three identified motifs resemble the canonical m^{6}A motif RRACH sequence (Additional file 2: Fig. S3).

We performed metagene profiling to examine the distribution of DMMPs within transcriptomes and found that both hyper- and hypomethylated m^{6}A peaks were highly enriched around the stop codon (Fig. 3b). Further examination of m^{6}A fraction in the five non-overlapping segments of transcripts revealed that the m^{6}A peaks in both hypo and hyper groups were dominantly enriched within 3'UTR (54.6% for hypo and 56.68% for hyper), CDS (25.92% and 23.14%) and around stop codon (13.19% and 11.02%) (Fig. 3c and Additional file 2: Fig. S2a). The majority of hypo- and hypermethylated transcripts were mRNAs (80.44% for hypo and 70.61% for hyper), and ~14-18% were lncRNA and the rest were other types of RNAs (Fig. 3d and Additional file 2: Fig. S2b).

The hypomethylated m^{6}A peak number in chRCC is 2-fold more than the hypermethylated peaks (Fig. 3a), in line with the finding that total identified m^{6}A peaks in chRCC are less than those in normal tissues (Fig. 2a). Therefore, we firstly focused on the hypomethylated m^{6}A peaks in chRCC. To explore the potential role of hypo-methylated m^{6}A peaks in chRCC, we took advantage of the algorithm DAVID to examine the most preferential expression tissues of m^{6}A hypomethylated genes. The results showed that m^{6}A hypomethylated genes were preferentially expressed in epithelium, followed by brain, placenta, and renal cell carcinoma (RCC) (Fig. 3e), indicating the correlation between these genes and RCC. We performed Gene Ontology (GO) enrichment analysis to uncover the functions of these genes. The results revealed that m^{6}A hypomethylated genes were enriched in many biological processes involved in kidney development and cancer pathogenesis, including transcription, androgen receptor signaling pathway, GTPase activity, and cell-cell adhesion (Fig. 3f). Pathway analysis showed that m^{6}A hypomethylated genes were mainly enriched in cancer-related pathways (Fig. 3g). These results suggested that the hypomethylated m^{6}A genes may participate in various pathophysiologic aspects of chRCC through different pathways.

We also explored the potential function of hypermethylated m^{6}A peaks in chRCC. The results showed that m^{6}A hypermethylated genes were preferentially expressed in brain, followed by epithelium, duodenum, fetal kidney, and ovary (Additional file 2: Fig. S2c). GO biological process analysis revealed that m^{6}A hypermethylated genes were significantly associated with protein phosphorylation, positive regulation of cholesterol efflux, ubiquinone biosynthetic process, regulation of mitophagy, and so on (Additional file 2: Fig. S2d). Pathway analysis showed that m^{6}A hypermethylated genes were mainly enriched in ubiquitin mediated proteolysis, metabolic pathways, and adherent junction (Additional file 2: Fig. S2e). Collectively, the results reveal both m^{6}A hypomethylated and hypermethylated genes are involved in many regulatory pathways, especially hypomethylated genes directly enriched in cancer pathways, indicating that dysregulation of m^{6}A could be a regulatory factor in the pathogenesis of chRCC.

The expression dysregulated genes in chRCC impair the normal functions of kidney

We next investigated the global mRNA expression patterns in normal and chRCC tissues by using the RNA-seq dataset (m^{6}A-SEAL-seq input library). The results showed that a total of 3,911 mRNAs were significantly dysregulated in chRCC of three subjects compared with normal tissues, including 2,344 downregulated mRNAs and 1,567 upregulated mRNAs (fold change ≥ 2, $p < 0.05$) (Fig. 4a). Hierarchical clustering depicted differential expression profiles in all the samples. (Fig. 4b).

We examined the preferentially expressed tissues of the dysregulated genes (3,911) using the algorithm DAVID. The result showed that the dysregulated genes were preferentially expressed in kidney, followed by liver and plasma (Fig. 4c), suggesting our data was reliable and these genes may participate in kidney development. We further performed GO analysis and KEGG pathway analysis. GO analysis revealed that the dysregulated genes were significantly enriched in metabolic process, transmembrane transport including sodium ion transport, oxidation-reduction process, excretion, kidney development, angiogenesis, and P450 pathway (Fig. 4d). In line with the result of GO, the KEGG analysis result also revealed that the dysregulated genes were significantly associated with multiple metabolic pathways including many amino acid metabolism or degradation, fatty acid degradation, cytochrome P450-related drug metabolism and xenobiotics metabolism (Fig. 4e). These results showed that the expression levels of around four thousand genes were dysregulated in chRCC, preliminarily illustrating that the dysregulated genes in chRCC impair the normal function of kidney, especially metabolic function.

New m^{6}A regulatory signature in the pathogenesis of chRCC

Considering that m^{6}A can either destabilize m^{6}A-modified transcripts through the recognition of YTHDF2 or stabilize m^{6}A-modified transcripts through the recognition of IGF2BP [14], we investigated the correlation between m^{6}A methylation levels and transcript levels. We overlapped the m^{6}A hypermethylated and hypomethylated genes with the differentially expressed genes. In 593 hypermethylated genes, 44 genes were downregulated and 68 genes were upregulated in chRCC tissues (Fig. 5a left). In 1,137 hypomethylated genes, 123 genes were downregulated and 51 genes were upregulated (Fig. 5a right). We next took the m^{6}A hypermethylated and hypomethylated genes as two

groups to analyze their transcript accumulation in chRCC and normal tissues. The result showed that the m^{6}A hypermethylated genes (ie. transcripts with higher m^{6}A levels) tended to preferentially exhibit upregulated transcription levels in chRCC (Fig. 5b), revealing the positive correlation between m^{6}A methylation levels and transcript levels in chRCC. Note we found that the expression of *YTHDF2* transcript was downregulated in chRCC (Fig. 1c). The positive correlation between m^{6}A levels and transcript levels in chRCC suggests m^{6}A in chRCC tends to affect gene regulation positively, potentially stabilizing m^{6}A-modified transcripts or escaping from YTHDF2-mediated mRNA decay pathway due to the lower expression YTHDF2 in chRCC.

To further analyze the role of DMMGs in cancers, we intersected DMMGs with Cancer Gene Census (CGC) database [50], a database consists of genes with strong indications of a role in cancer, and found that 73 and 23 genes were annotated in the hypomethylated and hypermethylated genes separately (Additional file 1: Dataset S2 and Dataset S3). Among these cancer-related genes, 10 genes were differentially expressed genes, including NOCH1 and FGFR1. NOTCH1 plays distinct roles in different cancers: NOTCH1 functions as a tumor suppressor gene in mouse skin and oral squamous cell carcinoma (OSCC) [51], and the expression of *NOTCH1* is decreased significantly in these cancer tissues [52]; whereas in Glioma and colon cancer, NOTCH1 functions as an oncogene and its expression level is increased in these two cancer tissues [53-55]. According to Integrative Genomics Viewer (IGV) software, the m^{6}A modification level in *NOTCH1* transcript was decreased significantly in chRCC compared to normal tissues (Fig. 5c left) and qPCR results in six patients showed the transcript expression level of *NOTCH1* was reduced significantly in chRCC tissue (Fig. 5c right). The downregulated expression of *NOTCH1* in chRCC is consistent with its expression pattern in mouse skin and OSCC cancers, suggesting NOTCH1 might act as a tumor suppressor in chRCC. Fibroblast growth factor receptor 1 (FGFR1) is a known oncogene. In breast cancer, the expression level of FGFR1 shows positive correlation with the amplification of cancer cell [56-58]. In lung cancer models, activation of FGFR1 promotes proliferation and migration of tumor cell while inhibition of FGFR1 suppresses tumor growth [59]. We found the m^{6}A methylation level of *FGFR1* was significantly decreased and the transcript expression level of *FGFR1* was increased in chRCC tissue (Fig. 5d right), which strongly suggests FGFR1 is an oncogene in chRCC similar to that in breast cancer and lung cancer.

We conducted principal component analysis of the differential expressed DMMGs in 65 chRCC cases from The Cancer Genome Atlas (TCGA) database. Based on the expression of these genes, we could completely distinguish chRCC samples from normal samples (Fig. 5e). Cox regression screen and least absolute shrinkage and selection operator (LASSO) identified three m^{6}A-dependent signatures **(**Additional file 1: Dataset S4**)** and defined a m^{6}A-dependent cox model in the training set (Additional file 2: Fig. S4a). Concordance index (C-index = 0.96) showed that the proposed model has a high prognostic power. In this model, we separated patients into high-risk or low-risk group according to their risk score, and patients with different 5-years survival could be distinguished completely between the two groups (Log-rank $p < 0.0001$) (Fig. 5f). AUC of ROC curve also confirmed the prognostic power of the m^{6}A-dependent model (Additional file 2: Fig. S4b). Then the proposed model was applied to the testing set for prediction.

We calculated risk score of each patient in the testing set and assigned to high-risk or low-risk group according to the cut off value in the training set. The Kaplan-Meier survival curve and log-rank between the two groups showed significant difference (Fig. 5g), which demonstrated the high predictive ability of the m^{6}A-dependent model. Furthermore, we also test the m^{6}A-dependent model in ccRCC samples (a cohort of 602 cases from TCGA database) and PRCC dataset (a cohort of 318 cases from TCGA database). The results indicated that the m^{6}A-dependent model is also suitable for ccRCC, but not PRCC (Additional file 2: Fig. S4c, d).

Discussion

Although the incidence and mortality of chRCC is the least among the three types of kidney cancer, there are still nearly thousands of people died owing to chRCC all of the world according to GCO statistic in 2020. Thereby, the underlying mechanism for adjuvant therapy is needed. Over the past few years, an increasing amount of efforts have been tried to illustrate the mechanism of m^{6}A modification in RCC, leading to extensive accumulation about the correlation between m^{6}A modification and RCC. However, these researches mainly focused on ccRCC and RPCC, while chRCC were rarely studied. Here, we demonstrated that m^{6}A writer WTAP and m^{6}A erasers FTO and ALKBH5 were downregulated in chRCC tissues. Consistently, our m^{6}A-SEAL-seq in three subjects of chRCC and corresponding tumor-adjacent normal tissues identified 644 hypermethylated m^{6}A peaks representing 593 transcripts and 1,304 hypomethylated m^{6}A peaks representing 1,137 transcripts in chRCC tissues, which could be directly induced by the aberrant expression of WTAP and FTO/ALKBH5. Further functional studies showed that genes with hyper- or hypomethylated peaks were mainly enriched in kidney development and cancer pathogenesis related pathway, which is a further proof of the fundamental role of m^{6}A modification in chRCC. We also found m^{6}A reader *YTHDF2* were downregulated in chRCC tissues. YTHDF2 is a well-studied m^{6}A reader and functions in m^{6}A-dependent gene regulation by affecting RNA stability [12, 60–63], suggesting there is an m^{6}A-dependent RNA degradation and gene dysregulation in chRCC. Cumulative fraction of RNA transcript accumulation between the m^{6}A hypermethylated genes and hypomethylated genes revealed the positive correlation between m^{6}A methylation levels and transcript levels in chRCC, which may be caused by m^{6}A-mediated mRNA stabilization or escaping from YTHDF2-mediated mRNA decay pathway due to the lower expression YTHDF2 in chRCC.

Our RNA-seq results identified 2,344 downregulated mRNAs and 1,567 upregulated mRNAs. The GO and KEGG analysis of these dysregulated genes revealed that chRCC impairs the normal function of kidney, especially in metabolism. By CGC database analysis [50], we found 96 genes with differential m^{6}A methylation levels (DMMGs) were causally implicated in cancers, including 73 hypomethylated genes and 23 hypermethylated genes in chRCC. Among them, *ZEB1* as an oncogene and *PBRM1*, *ASXL2* and *SETD2* as tumor suppressor genes. Combined with our RNA-seq data, we found 10 cancer-related DMMGs were differential expressed in chRCC, including *NOTCH1* and *FGFR1*. The m^{6}A methylation level at 3'UTR of *NOTCH1* and the transcript expression level of *NOTCH1* were significantly reduced in chRCC.

The m^{6}A methylation level at 3'UTR of *FGFR1* was also decreased, but the expression level of *FGFR1* was increased significantly. Considering previous functions of NOTCH1 and FGFR1 in other cancers, our results suggest that NOTCH1 and FGFR1 might respectively act as a tumor suppressor and an oncogene in chRCC. Base our preliminary results, we proposed a potential m^{6}A regulatory role in pathogenesis of chRCC, where the downregulated m^{6}A writer subunit WTAP in chRCC reduces m^{6}A levels in *NOTCH1* and *FGFR1*, leading to the decreased *NOTCH1* expression and the upregulated *FGFR1* expression through m^{6}A-mediated post-transcriptional gene regulation. Further functional studies are needed to clarify the molecular mechanisms of above-mentioned genes in the development of chRCC.

Based on the significant prognostic signatures identified from the cox regression and LASSO analysis in training set, we build a m^{6}A-dependent prognostic model. With benign performance in testing data, this prognostic model shows excellent predictive ability of the survival outcome, even in ccRCC. These results indicated the m^{6}A-dependent prognostic model could be used to comprehensively evaluate the survival outcome of chRCC patients and ccRCC patients in clinical practice.

Conclusion

This study presented the first m^{6}A transcriptome-wide profile of human chRCC, which provide a potential link between abnormal m^{6}A RNA modifications and cancer-related gene expressions. We hope it can be helpful for the m^{6}A methylation-based research on chRCC epitranscriptomic etiology and pathogenesis.

Abbreviations

GCO: Global Cancer Observatory; ccRCC: clear cell renal cell carcinoma; pRCC: papillary renal cell carcinoma; chRCC: chromophobe renal cell carcinoma; m^{6}A**:** *N*^{6}-methyladenosine; mRNA: Messenger RNA; METTL3/14: methyltransferase-like 3/14; WTAP: Wilms' tumor 1 (WT1)-associating protein; FTO: Fat Mass and Obesity-associated protein; ALKBH5: human AlkB homolog 5; YTHDF2: YTH domain family protein 2 ; HNRNPC: heterogeneous nuclear ribonucleoproteins C; IGF2BP3: Insulin-like growth factor 2 mRNA binding protein 3; FDR: false discovery rate; MeRIP-Seq: Methylated RNA Immunoprecipitation Next Generation Sequencing; CDS: Coding sequences; 3'UTR: 3' untranslated region; DMMPs: Differentially methylated m^{6}A peaks; lncRNA: Long non-coding RNA; GO: Gene Ontology; KEGG: Kyoto Encyclopedia of Genes and Genomes; CGC: Cancer Gene Census; OSCC: oral squamous cell carcinoma; IGV: Integrative Genomics Viewer; FGFR1: Fibroblast growth factor receptor 1.

Declarations

Ethics approval and consent to participate

The study has been approved by the ethics committee of the Peking University Third Hospital, and each participant has signed written informed consent.

Consent for publication

Not applicable.

Availability of data and materials

The raw sequence data of RNA-seq (input), m^6A-SEAL-seq have been deposited in the Genome Sequence Archive in the National Genomics Data Center (NGDC), Beijing Institute of Genomics, Chinese Academy of Sciences, under accession number (PRJCA004912).

Competing interests

The authors declare no competing interests.

Funding

This work was supported by the National Basic Research Program of China (2019YFA0802201 and 2017YFA0505201), the National Natural Science Foundation of China (nos. 21822702, 21820102008, 92053109, and 21432002), and Beijing Natural Science Foundation (Z200010).

Authors' contributions

CZG, JGF and MLL designed the study; YJB, ZW, QY, ZN and CZX performed the experiments; YJB and ZW analyzed the data; YJB, ZW and LM prepared the figures; CZG, YJB and ZW contributed to drafting the manuscript; GLY and LC revised the manuscript; JGF and MLL supervised this study. All authors read and approved the final manuscript.

Acknowledgements

Not applicable.

References

1. Jonasch E, Walker CL, Rathmell WK. Clear cell renal cell carcinoma ontogeny and mechanisms of lethality. Nat Rev Nephrol. 2021;17(4):245-61.
2. O. Martínez-Sáez, P. Gajate Borau, T. Alonso-Gordoa, J. Molina-Cerrillo, E. Grande. Targeting HIF-2 α in clear cell renal cell carcinoma: A promising therapeutic strategy. Crit Rev Oncol Hematol. 2017; 111: 117-23.
3. Atkins MB, Tannir NM. Current and emerging therapies for first-line treatment of metastatic clear cell renal cell carcinoma. Cancer Treat Rev. 2018; 70:127-37.
4. Wolf MM, Kimryn Rathmell W, Beckermann KE. Modeling clear cell renal cell carcinoma and therapeutic implications. Oncogene. 2020;39(17):3413-26.
5. McCroskey Z, Sim SJ, Selzman AA, Ayala AG, Ro JY. Primary collision tumors of the kidney composed of oncocytoma and papillary renal cell carcinoma: A review. Ann Diagn Pathol. 2017;

29:32-6.

6. Rogala J, Kojima F, Alaghehbandan R, Agaimy A, Martinek P, Ondic O, et al. Papillary renal cell carcinoma with prominent spindle cell stroma - tumor mimicking mixed epithelial and stromal tumor of the kidney: Clinicopathologic, morphologic, immunohistochemical and molecular genetic analysis of 6 cases. Ann Diagn Pathol. 2020;44:151441.
7. Moch H, Cubilla AL, Humphrey PA, Reuter VE, Ulbright TM. The 2016 WHO Classification of Tumours of the Urinary System and Male Genital Organs-Part A: Renal, Penile, and Testicular Tumours. Eur Urol. 2016;70(1):93-105.
8. Cancer Genome Atlas Research Network. Comprehensive molecular characterization of clear cell renal cell carcinoma. Nature. 2013; 499(7456):43-9.
9. Volpe A, Novara G, Antonelli A, Bertini R, Billia M, Carmignani G, et al. Chromophobe renal cell carcinoma (RCC): oncological outcomes and prognostic factors in a large multicentre series . BJU Int. 2012;110(1):76-83.
10. Przybycin CG, Cronin AM, Darvishian F, Gopalan A, Al-Ahmadie HA, Fine SW, et al. Chromophobe renal cell carcinoma: a clinicopathologic study of 203 tumors in 200 patients with primary resection at a single institution. Am J Surg Pathol. 2011;35(7):962-70.
11. Cantara WA, Crain PF, Rozenski J, McCloskey JA, Harris KA, Zhang X, et al. The RNA Modification Database, RNAMDB: 2011 update. Nucleic Acids Res. 2011;39(Database issue): D195-D201.
12. Wang X, Lu Z, Gomez A, Hon GC, Yue Y, Han D, et al. N6-methyladenosine-dependent regulation of messenger RNA stability. Nature. 2014;505(7481):117-20.
13. Wei LH, Song P, Wang Y, Lu Z, Tang Q, Yu Q, et al. The m^6A Reader ECT2 Controls Trichome Morphology by Affecting mRNA Stability in Arabidopsis. Plant Cell. 2018;30(5):968-85.
14. Huang H, Weng H, Sun W, Qin X, Shi H, Wu H, et al. Recognition of RNA N6-methyladenosine by IGF2BP proteins enhances mRNA stability and translation, Nat. Cell Biol; 2018; 20(3): 285–95.
15. Hou Y, Sun J, Wu B, Gao Y, Nie H, Nie Z, et al. CPSF30-L-mediated recognition of mRNA m6A modification controls alternative polyadenylation of nitrate signaling-related gene transcripts in Arabidopsis. Mol Plant. 2021;14(4):688-99.
16. Song P, Yang J, Wang C, Lu Q, Shi L, Tayier S, et al. Arabidopsis N6-methyladenosine reader CPSF30-L recognizes FUE signals to control polyadenylation site choice in liquid-like nuclear bodies. Mol Plant. 2021;14(4):571-87.
17. Horiuchi K, Kawamura T, Iwanari H, Ohashi R, Naito M, Kodama T, et al. Identification of Wilms' tumor 1-associating protein complex and its role in alternative splicing and the cell cycle. J Biol Chem. 2013;288(46):33292-302.
18. Xiao W, Adhikari S, Dahal U, Chen YS, Hao YJ, Sun BF, et al. Nuclear m6A reader YTHDC1 regulates mRNA splicing. Mol Cell; Mol Cell. 2016;61(4):507-19.
19. Barbieri I, Tzelepis K, Pandolfini L, Shi J, Millán-Zambrano G, Robson SC, et al. Promoter-bound METTL3 maintains myeloid leukaemia by m6A-dependent translation control. Nature.

2017;552(7683):126-31.

20. Wang X, Zhao BS, Roundtree IA, Lu Z, Han D, Ma H, et al. N(6)-methyladenosine Modulates Messenger RNA Translation Efficiency. Cell. 2015;161(6):1388-99.
21. Bokar JA, Shambaugh ME, Polayes D, Matera AG, Rottman FM. Purification and cDNA cloning of the AdoMet-binding subunit of the human mRNA (N6-adenosine)-methyltransferase. RNA. 1997;3(11):1233-47.
22. Liu J, Yue Y, Han D, Wang X, Fu Y, Zhang L, et al. A METTL3-METTL14 complex mediates mammalian nuclear RNA N6-adenosine methylation. Nat Chem Biol. 2014;10(2):93-5.
23. Yang Y, Hsu PJ, Chen YS, Yang YG. Dynamic transcriptomic m6A decoration: writers, erasers, readers and functions in RNA metabolism. Cell Res. 2018;28(6):616-24.
24. Ping XL, Sun BF, Wang L, Xiao W, Yang X, Wang WJ, et al. Mammalian WTAP is a regulatory subunit of the RNA N6-methyladenosine methyltransferase. Cell Res. 2014;24(2):177-89.
25. Agarwala SD, Blitzblau HG, Hochwagen A, Fink GR. RNA methylation by the MIS complex regulates a cell fate decision in yeast. PLoS Genet. 2012;8(6): e1002732.
26. Jia G, Fu Y, Zhao X, Dai Q, Zheng G, Yang Y, et al. N6-methyladenosine in nuclear RNA is a major substrate of the obesity-associated FTO. Nat Chem Biol. 2011;7(12):885-7.
27. Zheng G, Dahl JA, Niu Y, Fedorcsak P, Huang CM, Li CJ, et al. ALKBH5 is a mammalian RNA demethylase that impacts RNA metabolism and mouse fertility. Mol Cell. 2013;49(1):18-29.
28. Zhang Z, Theler D, Kaminska KH, Hiller M, de la Grange P, Pudimat R, et al. The YTH domain is a novel RNA binding domain. J Biol Chem. 2010;285(19):14701-10.
29. Xu C, Wang X, Liu K, Roundtree IA, Tempel W, Li Y, et al. Structural basis for selective binding of m6A RNA by the YTHDC1 YTH domain. Nat Chem Biol. 2014;10(11):927-9.
30. Li F, Zhao D, Wu J, Shi Y. Structure of the YTH domain of human YTHDF2 in complex with an m(6)A mononucleotide reveals an aromatic cage for m(6)A recognition. Cell Res. 2014;24(12):1490-2.
31. Liu T, Wei Q, Jin J, Luo Q, Liu Y, Yang Y, et al. The m6A reader YTHDF1 promotes ovarian cancer progression via augmenting EIF3C translation. Nucleic Acids Res. 2020;48(7):3816-31.
32. Chen Y, Peng C, Chen J, Chen D, Yang B, He B, et al. WTAP facilitates progression of hepatocellular carcinoma via m6A-HuR-dependent epigenetic silencing of ETS1. Mol Cancer. 2019;18(1):127.
33. He L, Li H, Wu A, Peng Y, Shu G, Yin G. Functions of N6-methyladenosine and its role in cancer. Mol Cancer. 2019;18(1):176.
34. Guo X, Li K, Jiang W, Hu Y, Xiao W, Huang Y, et al. RNA demethylase ALKBH5 prevents pancreatic cancer progression by posttranscriptional activation of PER1 in an m6A-YTHDF2-dependent manner. Mol Cancer. 2020;19(1):91.
35. Han J, Wang JZ, Yang X, Yu H, Zhou R, Lu HC, et al. METTL3 promote tumor proliferation of bladder cancer by accelerating pri-miR221/222 maturation in m6A-dependent manner. Mol Cancer. 2019;18(1):110.

36. Chen S, Zhang N, Zhang E, Wang T, Jiang L, Wang X, et al. A Novel m6A Gene Signature Associated With Regulatory Immune Function for Prognosis Prediction in Clear-Cell Renal Cell Carcinoma. Front Cell Dev Biol. 2021; 8:616972.
37. Wang Q, Zhang H, Chen Q, Wan Z, Gao X, Qian W. Identification of METTL14 in Kidney Renal Clear Cell Carcinoma Using Bioinformatics Analysis. Dis Markers. 2019; 2019: 5648783.
38. Zhou J, Wang J, Hong B, Ma K, Xie H, Li L, et al. Gene signatures and prognostic values of m6A regulators in clear cell renal cell carcinoma - a retrospective study using TCGA database. Aging (Albany NY). 2019;11(6):1633-47.
39. Sun Z, Jing C, Xiao C, Li T, Wang Y. Prognostic risk signature based on the expression of three m6A RNA methylation regulatory genes in kidney renal papillary cell carcinoma. Aging (Albany NY). 2020;12(21):22078-94.
40. Chen Y, Zhou C, Sun Y, He X, Xue D. m6A RNA modification modulates gene expression and cancer-related pathways in clear cell renal cell carcinoma. Epigenomics. 2020;12(2):87-99.
41. Wang Y, Xiao Y, Dong S, Yu Q, Jia G. Antibody-free enzyme-assisted chemical approach for detection of N6-methyladenosine. Nat Chem Biol. 2020;16(8):896-903.
42. Martin M. CUTADAPT removes adapter sequences from high-throughput sequencing reads. Embnet Journal. 2011; 17(1).
43. Pertea M, Kim D, Pertea GM, Leek JT, Salzberg SL. Transcript-level expression analysis of RNA-seq experiments with HISAT, StringTie and Ballgown. Nat Protoc. 2016;11(9):1650-67.
44. Zhang Y, Liu T, Meyer CA, Eeckhoute J, Johnson DS, Bernstein BE, et al. Model-based analysis of ChIP-Seq (MACS). Genome Biol. 2008;9(9): R137.
45. Heinz S, Benner C, Spann N, Bertolino E, Lin YC, Laslo P, et al. Simple combinations of lineage-determining transcription factors prime cis-regulatory elements required for macrophage and B cell identities. Mol Cell. 2010;38(4):576-89.
46. Cui X, Zhang L, Meng J, Rao MK, Chen Y, Huang Y. MeTDiff: A Novel Differential RNA Methylation Analysis for MeRIP-Seq Data. IEEE/ACM Trans Comput Biol Bioinform. 2018;15(2):526-34.
47. Love MI, Huber W, Anders S. Moderated estimation of fold change and dispersion for RNA-seq data with DESeq2. Genome Biol. 2014;15(12):550.
48. Zhang H, Shi X, Huang T, Zhao X, Chen W, Gu N, et al. Dynamic landscape and evolution of m6A methylation in human. Nucleic Acids Res. 2020;48(11):6251-64.
49. Ramírez F, Dündar F, Diehl S, Grüning BA, Manke T. deepTools: a flexible platform for exploring deep-sequencing data. Nucleic Acids Res. 2014;42(Web Server issue): W187-W91.
50. Sondka Z, Bamford S, Cole CG, Ward SA, Dunham I, Forbes SA. The COSMIC Cancer Gene Census: describing genetic dysfunction across all human cancers. Nat Rev Cancer. 2018;18(11):696-705.
51. Nicolas M, Wolfer A, Raj K, Kummer JA, Mill P, van Noort M, et al. Notch1 functions as a tumor suppressor in mouse skin. Nat Genet. 2003;33(3):416-21.

52. Rangarajan A, Talora C, Okuyama R, Nicolas M, Mammucari C, Oh H, et al. Notch signaling is a direct determinant of keratinocyte growth arrest and entry into differentiation. EMBO J. 2001;20(13):3427-36.
53. Ishiguro H, Okubo T, Kuwabara Y, Kimura M, Mitsui A, Sugito N, et al. NOTCH1 activates the Wnt/β-catenin signaling pathway in colon cancer. Oncotarget. 2017;8(36):60378-89.
54. Zhou P, Wang C, Hu Z, Chen W, Qi W, Li A. Genistein induces apoptosis of colon cancer cells by reversal of epithelial-to-mesenchymal via a Notch1/NF-κB/slug/E-cadherin pathway. BMC Cancer. 2017;17(1):813.
55. Li J, Li Q, Lin L, Wang R, Chen L, Du W, et al. Targeting the Notch1 oncogene by miR-139-5p inhibits glioma metastasis and epithelial-mesenchymal transition (EMT). BMC Neurol. 2018;18(1):133.
56. Turner N, Pearson A, Sharpe R, Lambros M, Geyer F, Lopez-Garcia MA, et al. FGFR1 amplification drives endocrine therapy resistance and is a therapeutic target in breast cancer. Cancer Res. 2010;70(5):2085-94.
57. Katoh M. FGFR inhibitors: Effects on cancer cells, tumor microenvironment and whole-body homeostasis (Review). Int J Mol Med. 2016;38(1):3-15.
58. Drago JZ, Formisano L, Juric D, Niemierko A, Servetto A, Wander SA, et al. FGFR1 Amplification Mediates Endocrine Resistance but Retains TORC Sensitivity in Metastatic Hormone Receptor-Positive (HR+) Breast Cancer. Clin Cancer Res. 2019;25(21):6443-51.
59. Wang K, Ji W, Yu Y, Li Z, Niu X, Xia W, et al. FGFR1-ERK1/2-SOX2 axis promotes cell proliferation, epithelial-mesenchymal transition, and metastasis in FGFR1-amplified lung cancer. Oncogene. 2018;37(39):5340-54.
60. Chen M, Wei L, Law CT, Tsang FH, Shen J, Cheng CL, et al. RNA N6-methyladenosine methyltransferase-like 3 promotes liver cancer progression through YTHDF2-dependent posttranscriptional silencing of SOCS2. Hepatology. 2018; 67(6):2254-70.
61. Du H, Zhao Y, He J, Zhang Y, Xi H, Liu M, et al. YTHDF2 destabilizes m(6)A-containing RNA through direct recruitment of the CCR4-NOT deadenylase complex. Nat Commun. 2016;7: 12626.
62. Huang T, Liu Z, Zheng Y, Feng T, Gao Q, Zeng W. YTHDF2 promotes spermagonial adhesion through modulating MMPs decay via m6A/mRNA pathway. Cell Death Dis. 2020;11(1):37.
63. Liu J, Gao M, Xu S, Chen Y, Wu K, Liu H, et al. YTHDF2/3 Are Required for Somatic Reprogramming through Different RNA Deadenylation Pathways. Cell Rep. 2020;32(10):108120.

Figures

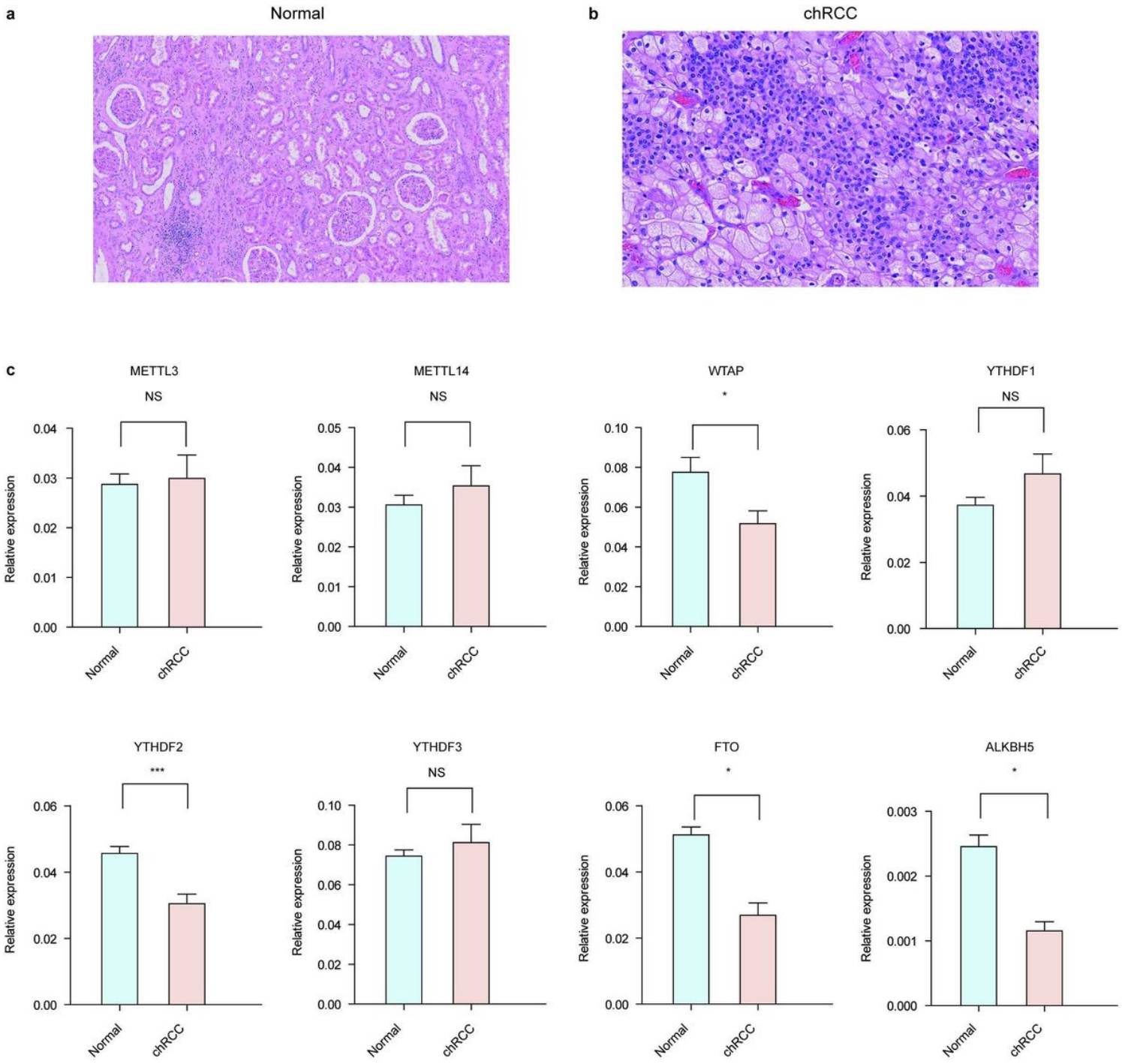

Figure 1

Hematoxylin and eosin (HE) staining and relative expression level of known m6A-related genes in normal and chRCC tissues by qPCR. a HE staining in normal tissues. b HE staining in chRCC tissues. c Relative expression level of METLL3, METTL14, WTAP, YTHDF1, YTHDF2, YTHDF3, FTO and ALKBH5. Data are presented as means ± SE, n = 6 biological replicates. *p < 0.05 (two-sided), * * * p < 0.005 (two-sided).

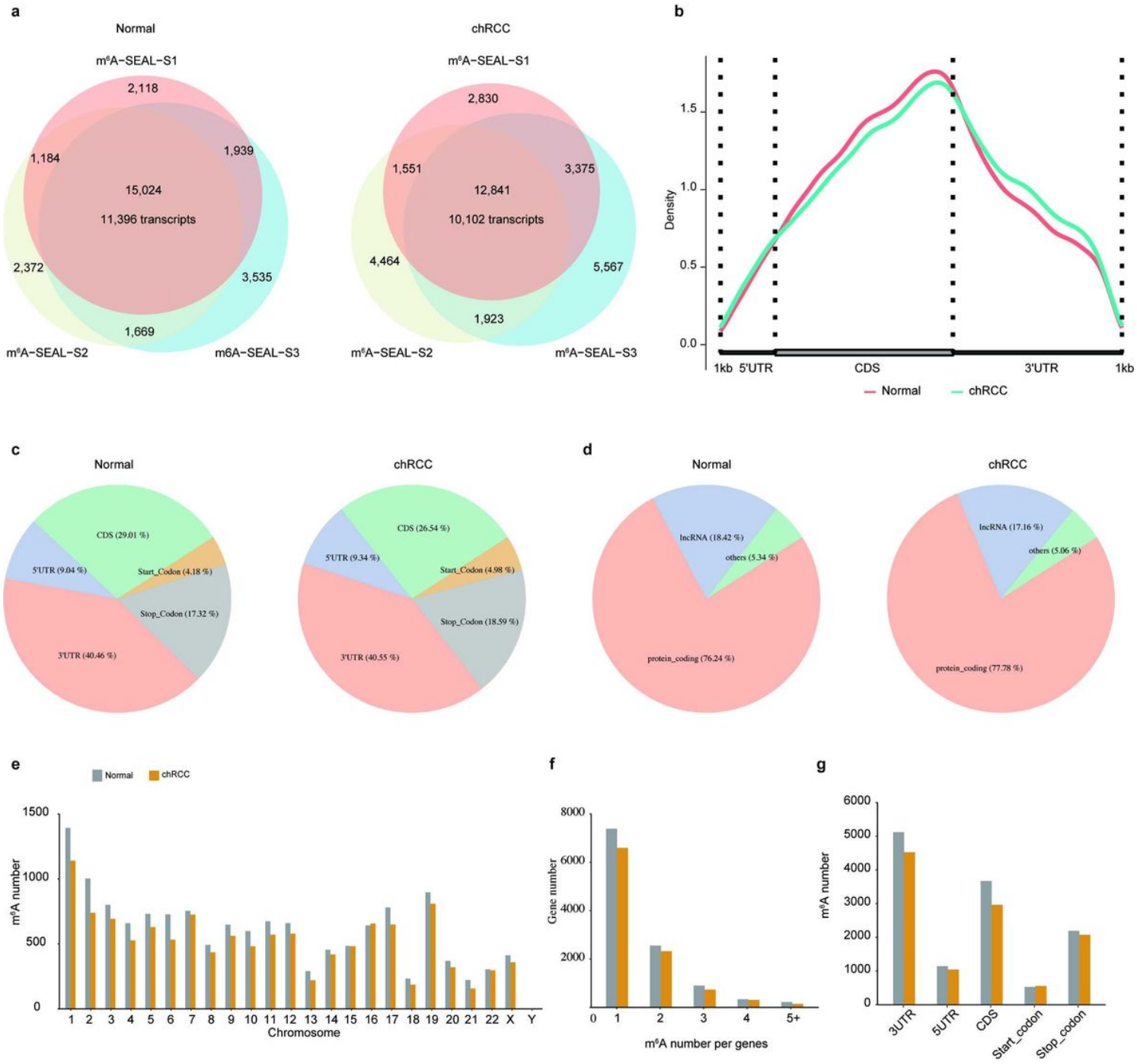

Figure 2

Characterization of m6A modification in normal and chRCC tissues reveals decreased methylation numbers in chRCC tissues. a Overlap of three biological replicates of m6A-SEAL-seq peaks in normal and chRCC tissues. b Metagene profile illustrating the region distribution of m6A peaks across the indicated mRNA segments. c Pie chart depicting the fraction of confident m6A peaks in each of the five non-overlapping transcript segments (5'UTR, start codon, coding sequence [CDS], stop codon and 3'UTR) in normal and chRCC tissues. d Pie chart depicting RNA types of m6A peaks in normal and chRCC tissues. e The number of m6A peaks in human chromosomes. f The number of m6A peaks per gene. g The number of m6A peaks in five non-overlapping transcript segments.

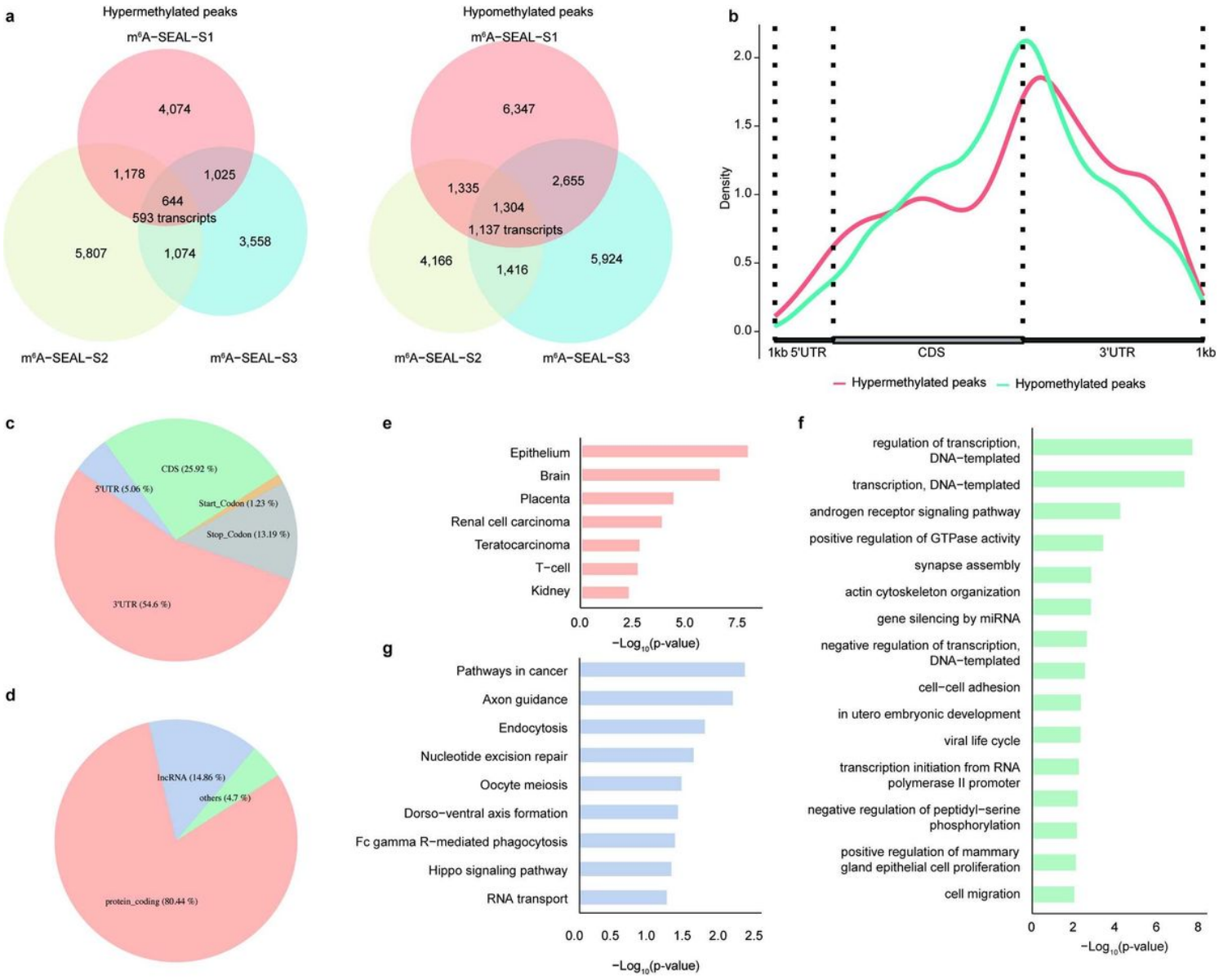

Figure 3

Tissue analysis, Gene Ontology (GO), and Kyoto Encyclopedia of Genes and Genomes (KEGG) analyses of hypomethylated genes in chRCC tissues. a Overlap of three biological replicates of hypermethylated (left) and hypomethylated (right) m6A peaks in chRCC tissues. b Metagene profile illustrating the region distribution of hypermethylated and hypomethylated m6A peaks across the indicated mRNA segments. c Pie chart presenting the fraction of the confident hypomethylated m6A peaks across five non-overlapping transcript segments. d Pie chart presenting RNA types (that is, transcript species) of the confident hypomethylated m6A peaks identified in chRCC. e-g UP_TISSUE (e), Gene ontology (GO) (f) and KEGG (g) analysis of the hypomethylated m6A genes.

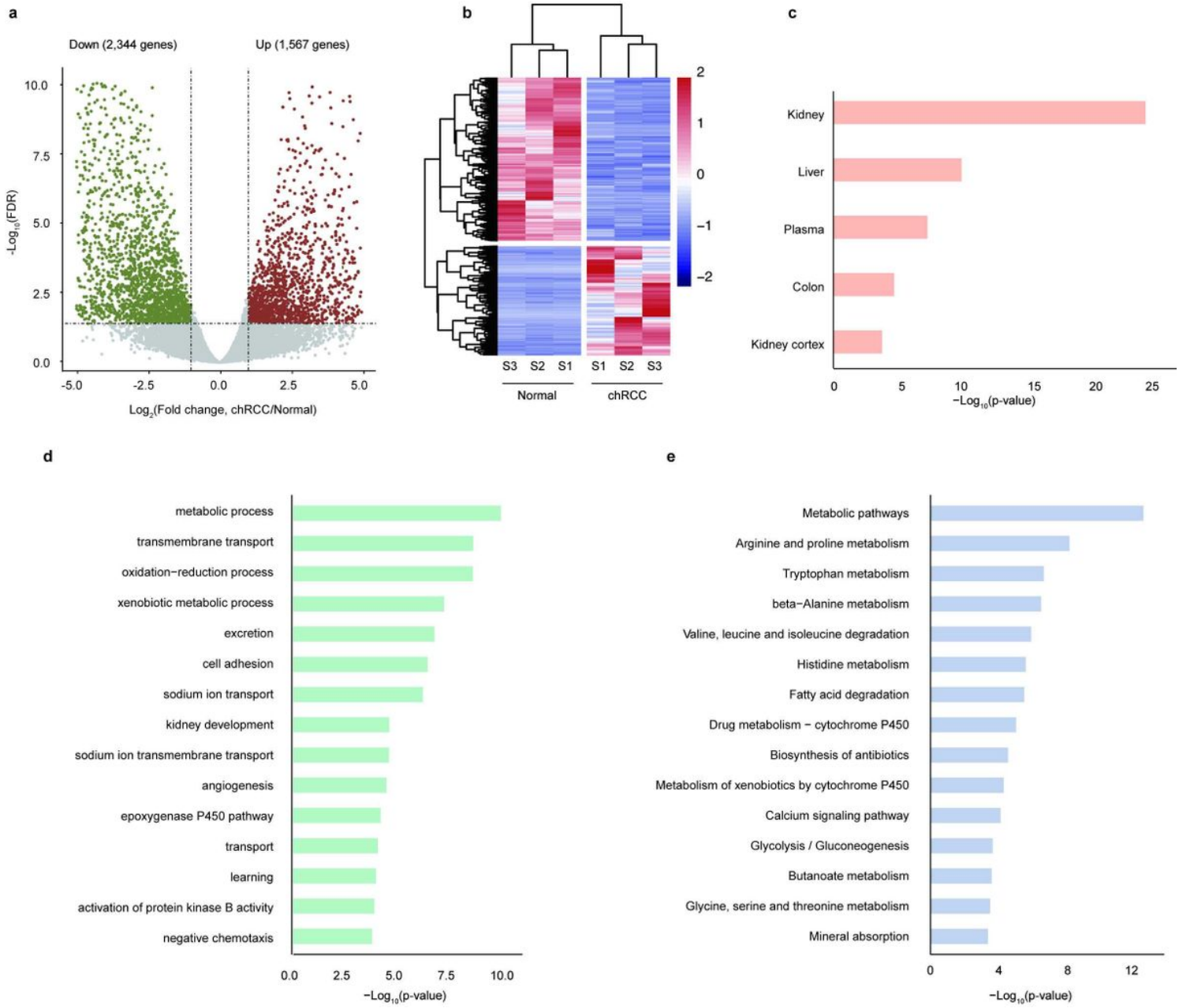

Figure 4

Differential expression genes in chRCC tissues compared with normal tissues. a Volcano plots showing the differentially expressed genes in chRCC tissues compared with those in adjacent normal tissues. b Heatmap plots showing the differentially expressed genes in chRCC tissues vs those in normal tissues. c-e UP_TISSUE (c), Gene ontology (GO) (d) and KEGG (e) analysis of the differential expression genes.

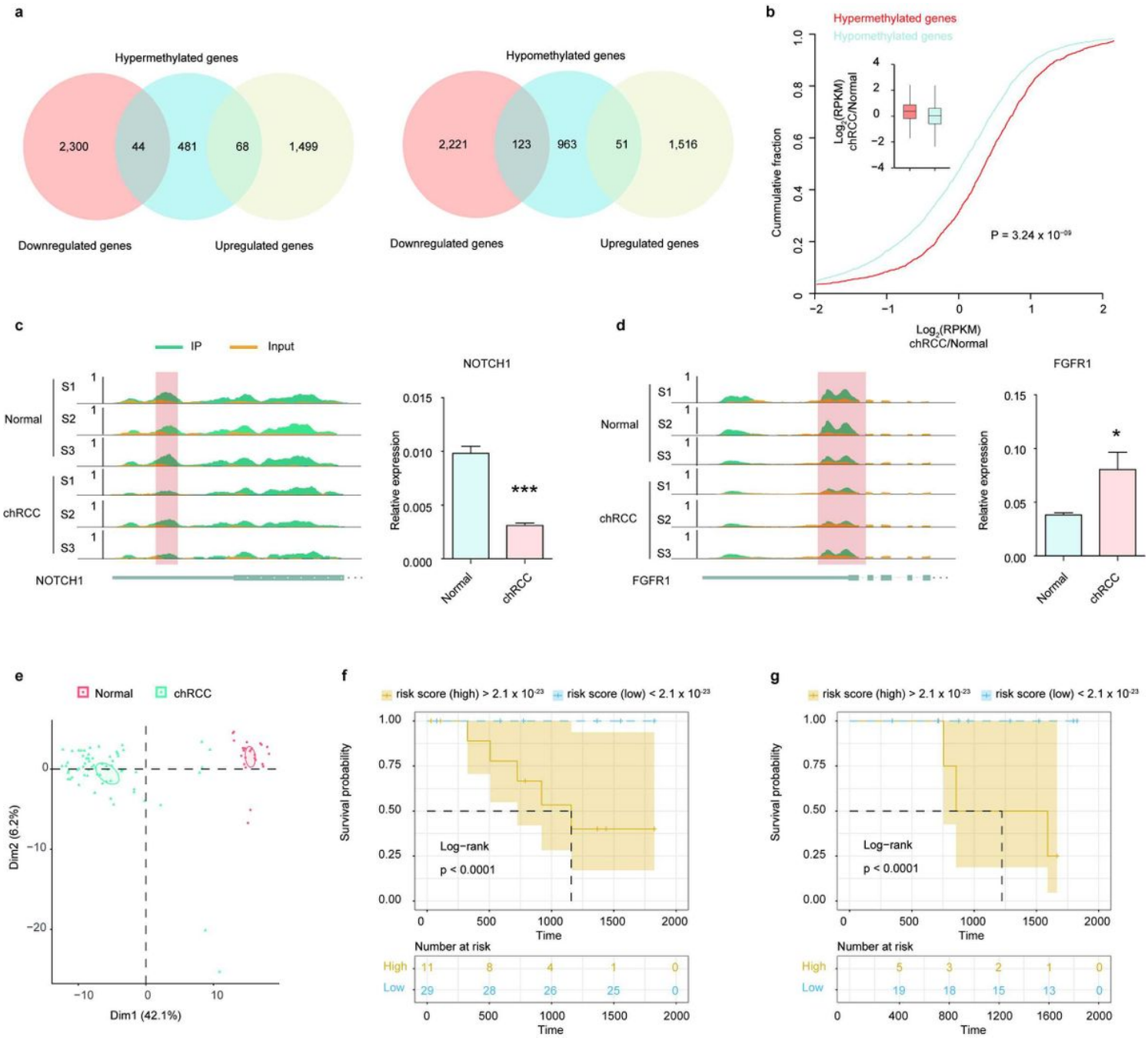

Figure 5

Conjoint analysis of m6A-SEAL-seq and RNA-seq data. a Overlap of hypermethylated genes with upregulated genes and downregulated genes (left). Overlap of hypomethylated genes with upregulated genes and downregulated genes (right). b Cumulative distribution displaying the expression level changes in mRNAs with hypermethylated or hypomethylated m6A modification. c, d Integrative genomics viewer (IGV) tracks showing the indicated m6A-SEAL-seq reads distribution on target transcripts and the relative expression level in normal and chRCC tissues: (c) NOTCH1, (d) FGFR1. e Principal component analysis for the expression profiles (fpkm-uq) of the differential expressed DMMGs to distinguish tumors from normal samples in chRCC cohort (from The Cancer Genome Atlas database). f, g Survival analyses

in the training set (f) and testing set (g). Log-rank p < 0.0001 showed a significant survival difference between the two sub-groups.

Supplementary Files

This is a list of supplementary files associated with this preprint. Click to download.

- Additionalfile1.xlsx
- Additionalfile2.rar